# Geometry of magnetosonic shocks and plane-polarized waves: Coplanarity Variance Analysis (CVA)

J. D. Scudder

Department of Physics and Astronomy, University of Iowa, Iowa City, Iowa, USA

[1]  Minimum Variance Analysis (MVA) is frequently used for the geometrical organization of a time series of vectors. The Coplanarity Variance Analysis (CVA) developed in this paper reproduces the layer geometry involving coplanar magnetosonic shocks or plane-polarized wave trains (including normals and coplanarity directions) 300 times more precisely ($<0.1°$) than MVA using the same input data. The CVA technique exploits the eigenvalue degeneracy of the covariance matrix present at planar structures to find a consistent normal to the coplanarity plane of the fluctuations. Although Tangential Discontinuities (TDs) have a coplanarity plane, the eigenvalues of their covariance matrix are usually not degenerate; accordingly, CVA does not misdiagnose TDs as shocks or plane-polarized waves. Together CVA and MVA may be used to sort between the hypotheses that the time series is caused by a one-dimensional current layer that has magnetic disturbances that are (1) coplanar, linearly polarized (shocks/plane waves), (2) intrinsically helical (rotational/tangential discontinuities), or (3) neither 1 nor 2.

**Citation:**  Scudder, J. D. (2005), Geometry of magnetosonic shocks and plane-polarized waves: Coplanarity Variance Analysis (CVA), *J. Geophys. Res.*, *110*, A02202, doi:10.1029/2004JA010660.

## 1. Introduction

[2]  The search for geometry in space plasmas invariably focuses on sites of relatively abrupt reorientations of the magnetic field and other fluid variables. For historical reasons these structures were initially catalogued using magnetometer measurements and collectively called Directional Discontinuities (DD). DDs are caused by localized current layers usually modeled as planar sheets with spatial variation allowed only along the surface normal. Surveys of DDs were initially organized by the net angular rotation $\omega$ of **B** caused by the localized current. It has since been determined largely by Minimum Variance Analysis [*Sonnerup and Cahill*, 1968] that the geometry and classification of such DDs is susceptible to large errors unless $\omega > 30°$ and the ratio of intermediate to smaller eigenvalue exceeds 10. The DDs confirmed in space plasmas include the Tangential Discontinuity (TD); the Rotational Discontinuity (RD); and the Fast, Slow, and Intermediate shocks (FS, SS, IS).

[3]  Minimum Variance Analysis (MVA) was invented to survey time profiles of magnetometer data at the magnetopause, looking to differentiate a locally closed magnetopause in the form of TDs from locally open magnetopause layers in the form of RDs modeled as a one-dimensional sheet current layer [*Sonnerup and Cahill*, 1968]. MVA presumes the one-dimensional nature of the current sheet and uses Gauss's law to require that the projection of **B** along a to-be-determined direction $\hat{n}$ should be constant.

The assertion central to the technique is that the variance of that component of the field about its mean and constant value should yield the smallest variance. The MVA problem is an extremum problem, reducible to a $3 \times 3$ eigenvalue problem for a real symmetric (covariance) matrix whose positive eigenvalues are the variances of the field along the principal coordinate axes [*Sonnerup and Scheible*, 1998]. The minimum eigenvalue $\lambda_1$ determines a related eigenvector direction $\zeta_1$ which MVA identifies with the normal $\hat{n}$ to the current sheet. By theorem, the eigenvectors $\zeta_j$ of the covariance matrix of MVA can be constructed to be mutually orthogonal; they form a convenient basis to define a transformation from the original sensor coordinates to a "minimum variance" coordinate system. The ease of making such a transformation explains its frequent use in the literature, even in circumstances where it is manifestly inappropriate. Second to its ease is the fact by theorem that it always returns an answer even though it may be inappropriate or ill-founded.

[4]  A tacit assumption of MVA is that the eigenvalues of the covariance matrix only have one "smallest" or minimum eigenvalue. The sufficient test for this condition is usually reformulated by the requirement that $(\lambda_2/\lambda_1) \geq 10$, where 2(1) denotes the intermediate (minimum) eigenvalue. In the literature MVA is usually introduced without discussion of this eigenvalue ratio, simply by announcing data transformed in "the" minimum variance coordinates without a discussion of its pedigree. When the eigenvalue spread has been discussed in the past, samples of DDs with $\omega > 30°$ only rarely satisfy the sufficient eigenvalue condition given above. The recent study by *Knetter et al.* [2004] has shown

that there is an interrelationship between adequate eigenvalue ratio and angular excursion that are compatible with good geometry determination. What are these other DDs with low spreads in covariance eigenvalues and large $\omega$? The layers are surely current layers, since direction of **B** is observed to change. This paper begins by examining the other DDs besides those for which MVA was constructed.

[5] There are other current layers with spatial variation allowed in only one-dimensional: these DDs are the Plane-Polarized Waves (PPW) and shocks which have two distinct orthogonal directions where the projections of **B**(t) are constant. For these structures the variance along these directions could be equally expected to be simultaneously small. It is for these circumstances that the new technique of Coplanarity Variance Analysis (CVA) is introduced in this paper. As discussed below, such geometries should be used rather than those implied by MVA when the covariance eigenvalue ratio is not comparable to or above the sufficient lower limit of 10 discussed above.

[6] It will be developed that CVA can find the geometry of PPW/shocks without becoming distracted and misdiagnosing true TDs (that have certain planar attributes that are indeed different from those of PPW and shocks). Conversely, it is shown below that MVA is only well suited to the task of delineating geometry when looking at RDs and TDs. By simulation we demonstrate the corollaries: (1) MVA analysis of a wide range of shocks does a horrible job reconstructing their geometry, and (2) CVA operating on an RD or TD with angular rotations of more than $30°$ also does an equally poor job of reconstructing their geometry. In this way we demonstrate the sieving property of MVA and CVA and illustrate how these tools operating on DDs of unknown pedigree could differentiate them without confusing them. Separately, MVA and CVA affirm or deny disjoint hypotheses under a common assumption that the DD under analysis results from a one-dimensional (1-D) planar current sheet: (1) MVA: is the layer an RD or a TD?; (2) CVA: is the layer a PPW or a MHD shock wave? If neither hypothesis is affirmed, a third hypothesis must be considered: (3) is the sampled DD determined by current systems that cannot be confined to a plane?

## 2. Review of DD Properties

[7] The magnetic field vectors through an RD can be viewed as if they are arranged to partially cover the surface of a right elliptical cone, always possessing a constant, nonzero field component, $B_n$, along the altitude of the cone (c.f. illustrations in the works of *Burlaga et al.* [1977] and *Baumjohann and Treumann* [1996]). The magnetic field vectors through a TD can be viewed as laying on a right elliptical cone in the limit that the altitude vanishes, leaving the magnetic field layers to sweep out an elliptical arc in a plane perpendicular to the direction of its "vanished" altitude. Thus **B**(t) at TDs can be viewed as being "coplanar," while **B**(t) at a RD are not. In the plane perpendicular to their altitudes the projection of **B**(t), called a hodogram, looks remarkably similar for TDs and RDs, usually being the arc of an ellipse when low pass filtered. Tangential discontinuities occur at interfaces between plasmas with no communication except lateral stress balance; they lack field lines that connect the two sides of the sharpest currents.

Thus the projection of **B** along the direction, $n_{TD}$, of spatial variation in a TD should vanish; the normal $\tau_{TD}$ to the TD coplanarity plane (containing all the **B**(t) of the TD) is collinear with $n_{TD}$, implying that $n_{TD} \times \tau_{TD} = \pm1$.

[8] The magnetic field vectors through a Plane-Polarized Wave PPW lay in a plane that contains the direction of propagation, $k_{PPW}$, and the wave's plane-polarized but fluctuating components. The magnetic lines of force of such a PPW lay in a PPW "coplanarity" plane; the PPW coplanarity plane also contains $k_{PPW}$. The normal to the coplanarity plane, $\tau_{PPW}$, is perpendicular to $k_{PPW}$. In a 1-D current layer geometry the spatial variation of the plane-polarized wave is along **k**; in this circumstance Gauss's law guarantees that the component of **B**(t) along **k** must be conserved and $\hat{k}$ should be a direction of small variation of the magnetic field. However, because the wave disturbance is postulated to be a plane-polarized there are additional directions, namely $\pm\tau_{PPW}$, along which the projection of the magnetic field should vanish and also have small variation. Summarizing for a PPW we have the condition $\tau_{PPW} \times k_{PPW} = 0$, which clearly differentiates its coplanarity plane from the coplanarity plane of a TD where the analogous two quantities are collinear rather than orthogonal.

[9] All three shocks (FS, SS, IS) are made up of magnetic fields that almost everywhere are "coplanar" like the field samples of a PPW. This assumption is (briefly) violated in the actual current carrying layer of the shock [*Goodrich and Scudder*, 1984]. It is in this sense that shock waves also have two orthogonal directions where components of **B**(t) are expected to be nearly constant and whose variation about those constant values should also be small. If a minimum variance layer has a magnetic hodogram that is linearly organized, it has two orthogonal directions where small variations, $\lambda$s, can be anticipated. In lieu of additional information such layers may be either a linearly polarized TD that does not propagate or PPW/shocks that do; with either identification the common attribute is plane polarization. The implied normal for the structure will depend on the TD or PPW option selected. The existence in shocks and plane-polarized waves of two orthogonal directions where constant average fields are expected is the essential insight of the CVA approach to the geometry of these structures.

[10] Eigenvalues of the covariance matrix are coordinate invariant assays of the vector field, playing the same roles as the three moments of inertia for the inertia tensor of distributed bodies. When the vector field's covariance matrix has eigenvalues with multiplicities, it possesses a higher symmetry than vector fields that do not possess such multiplicities. In this sense the magnetic field about RDs and TDs are current layers of lower symmetry than shocks and PPW. Since any given magnetic line of force through an RD does not reside in a plane, such lines possess nonzero torsion; while TDs do not possess field lines than transit the current layer, they are comprised of parallel sheets of magnetic lines of force that are skew with respect to their neighbors on both sides of the current sheet plane. When either a TD or (RD) is transited by the spacecraft, the magnetic field appears to rotate in a plane perpendicular to the current sheet normal, sweeping out a spiral staircase with the horizontal (canted) treads being successive skew (nested corkscrew) field lines. RDs and TDs can both be
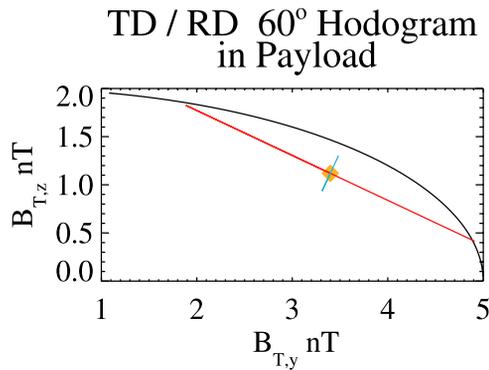
## TD / RD 60° Hodogram in Payload



**Figure 1.** Portrayal of the hodogram of a Tangential Discontinuity (TD) or Rotational Discontinuity (RD) in coordinates transverse to the adopted normal, illustrating the geometrical content of the direction of maximum (red) and intermediate variance (cyan) and the control on these segregated variances by the arc length of the net rotation of the hodogram. When the net angle $\omega$ of rotation of **B** gets small, the arc length of the hodogram is reduced and this curve increasingly approximates a linear segment, with ever-decreasing dispersion transverse to the direction of maximum variance. At some point this intermediate eigenvectors dispersion becomes comparable to the small dispersion along the normal and the eigenvalue problem is effectively degenerate. To avoid this "accidental" degeneracy, it is common practice to restrict geometry work with directional discontinuities to those with $\omega > 30°$.

viewed as essentially elliptically polarized layers, while shocks and PPW are essentially plane-polarized structures.

[11] RD/TD layers possess an elliptical polarization, while plane-polarized waves and shocks are higher symmetry structures with linear polarization. PPW and shocks are referred to below as Coplanar Wave Disturbances (CWDs). CWDs have magnetic tubes of force that are "almost everywhere" coplanar as they thread the current carrying layer and magnetically connect both sides of the current density. This paper identifies the higher symmetry of the CWD DDs as the reason why single spacecraft MVA determines a poor geometry for these layers; it also suggests a suitable computational approach for obtaining the geometry of CWDs in the form of Coplanarity Variance Analysis (CVA) that uses the same data input as MVA. CVA accurately ($\ll 1°$) reconstructs the shock normal (wavevector) and the orientation of the coplanarity (polarization) plane across a broad range of realistic slow and fast modeled shock profiles. Of course, CVA does not replace full Rankine-Hugoniot (R-H) fitting procedures [e.g., *Vinas and Scudder*, 1986] or multiple spacecraft assays [e.g., *Knetter et al.*, 2004] that rely on the augmented information of multiple diagnostics across the same shock or multiple spacecraft. CVA may, however, be the "best" available source of geometry for CWDs when the correlative measurements at a shock necessary to perform R-H tests or multiple spacecraft are unavailable at the requisite time resolution.

[12] The three eigenvectors of the covariance matrix organize the observed components of **B** and that of its hodogram determined by the locus of the components of **B**

transverse to the normal: $B_\perp(t) = \mathbf{B}(t) - (\mathbf{B}(t) \cdot \mathbf{n})\mathbf{n}$. The orientation of the intermediate and maximum eigenvalue's eigenvector in the plane of the hodogram are indicated in Figure 1 for a TD with net angular rotation of $\omega = 60°$. The measurement coordinate system is used to illustrate the typical elliptical motion of the hodogram that accompanies TD and RDs. The orientation of the maximum (intermediate) variance's eigenvector is indicated by the red (cyan) line segment. The half-length of each of these segments about the diamond is equal to the standard deviation determined from the respective eigenvalues of the covariance matrix. The diamond is located at the average transverse magnetic field components in this plane. The red direction of maximum variation (selected by the eigenvalue problem) is oriented to maximize the dispersion of the data projected along it. Conversely, the blue line is oriented so as to minimize the variance of the transverse components of **B** while being perpendicular to the red line. Clearly, the length of the arc is enhanced and the direction of maximum variance made more certain when the arc in the hodogram extends over a larger angle, a corollary of increasing $\omega$. An important observation, valid even as $\omega$ decreases, is that the direction of maximum variance still remains relatively well defined. If the transition at the TD/RD is accomplished by a very small $\omega$ such that a small portion of an arc will be well represented by a line segment, the intermediate (blue) dispersion will reduce to noise levels, artificially making the eigenvalue along the normal to this plane and along the cyan direction nearly equal with small eigenvalues. When this occurs, there is an "artificial" degeneracy in the DD sampled, rendering geometry from variance techniques of any type questionable for want of adequate leverage. This accidental degeneracy underlies the operational procedure of many years standing to not attempt to get geometry from DDs with angular changes that are too small.

## 3. Symptoms of the Problem

[13] An isomagnetic RD transition is illustrated in terms of its Cartesian components of **B** by the solid curves of Figure 2a. The coordinates were chosen so that the initial magnetic field direction was in the x-z plane. The normal component is shown in light blue (cyan), while the transverse components are illustrated in red (y) and green (z) traces. The dashed curve of the corresponding color is the arithmetic mean of that Cartesian component. Colored flags anchored by a diamond reflect the standard deviation of that component about its mean in this coordinate system. The normal component has a small variance. The other two components have variances that are larger owing to the coherent jumps in the averages of both of these components.

[14] Figure 2b illustrates the same RD of Figure 2a in the standard "minimum variance" coordinates where the MVA eigenvectors have become the new basis directions: $x' = \zeta_1$; $y' = \zeta_2$; and $z' = \zeta_3$. The standard deviations in the new coordinate system are also shown. The two Figures of Merit in the MVA panel are defined by FOM = $Q_1, Q_2$, where $Q_j = \lambda_j/(\lambda_1 + \lambda_2 + \lambda_3)$. By theorem, the sum of the variances cannot change under coordinate rotations. In the MVA coordinate system, however, the component variances in Figure 2a have been repartitioned among the transformed components of the magnetic field, increasing the variance of
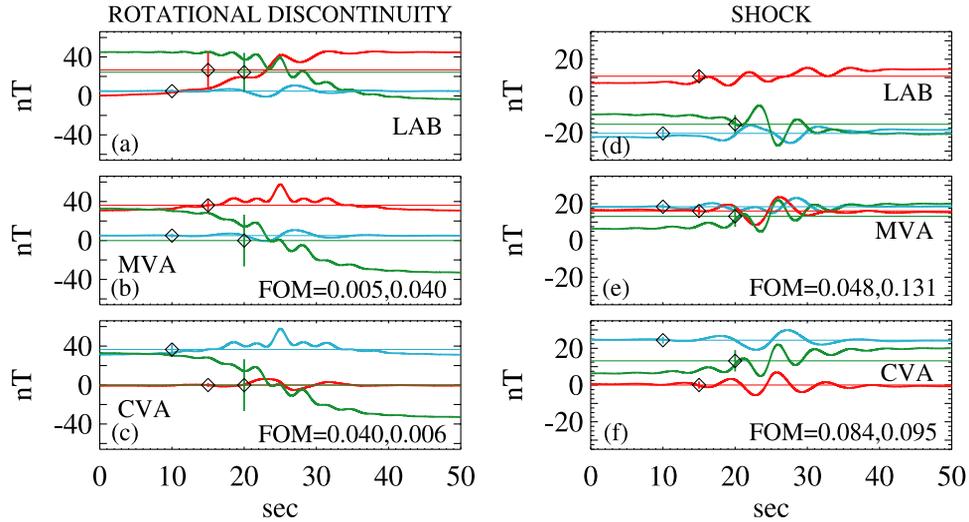
**Figure 2.** Left column pertains to simulated RD. Right column pertains to simulated Fast Shock. In both columns, thick curves depict the variation of three Cartesian components of **B** across time series. Light blue (x); two components transverse to x are illustrated in red (y) and green (z). Temporal average of each component is given by dashed line of the same color. Variance about the mean of each component is indicated by vertical error bar of the same color, anchored with a diamond on the average dotted line. FOM(1, 2) indicates $(\lambda_1, \lambda_2)/(\lambda_1 + \lambda_2 + \lambda_3)$. (a) RD with x direction along the normal. (b) Same RD as in Figure 2a described in MVA geometry: x along the minimum variance; z direction of maximum variance. (c) Same RD as in Figure 2a described in CVA geometry: y perpendicular to coplanarity plane, z in direction of maximum variance of MVA. (d) Fast Shock in laboratory coordinates. (e) Same Fast Shock as in Figure 2d but viewed in MVA geometry: x direction of minimum variance, z direction of maximum variance. (f) Same Fast shock as in Figure 2d in CVA geometry: y coplanarity plane normal, z maximum variance direction.

the $z'$ components, while compensating by lowering the variance along the $y'$ direction. Eigenvalues (variances) are (are not) coordinate invariant properties of the geometry. The ratio $\lambda_2/\lambda_1 = Q_2/Q_1 \sim 8$ in this example approaches the recommended [*Sonnerup and Scheible*, 1998] ratio of 10 for good geometry definition at TD/RDs using MVA. Since the variance is positive and it was already essentially 0 along **x**, it is not surprising that the minimum variance direction, $x'$, is selected parallel to **x** with essentially the same variance about it. (For the coordinate rotation between the two frames (Figure 2a $\rightarrow$ Figure 2b) the sum of the eigenvalues for eigenvectors transverse to the normal is also preserved as a corollary to the invariance of the sum of eigenvalues and the null variance along the x coordinates in both initial and final frames considered here.)

[15] The magnetic fields on either side of the shock, as sketched in Figure 3, should have no average components perpendicular to a yet to be found coplanarity plane, parallel to the two planes labeled C, C′. This plane also "contains" the shock normal **n**, the net vectorial changes of the magnetic field, and the fluid velocity, a property not shared by the coplanarity plane of a TD discussed above. The statements of "contain" and are "perpendicular" are in the sense of vector algebra of a vector field and MHD; these local geometrical statements do not imply the global geometrical properties of tubes of force that pierce the shock layer. For example, as the tube of magnetic force crosses the shock (S) layer, it migrates perpendicular to C (and thus the coplanarity plane) within the current carrying shock layer en route to the geometrically equivalent parts of "the"

coplanarity plane labeled C′ [cf. *Scudder*, 1995, Figure 15]. A plane-polarized wave train would have the same coplanar geometry, but the field lines throughout that disturbance would lay in one geometrical plane throughout the disturbance. If the normal to the coplanarity plane is identified as the $y''$ direction in CVA, there is the requirement in this
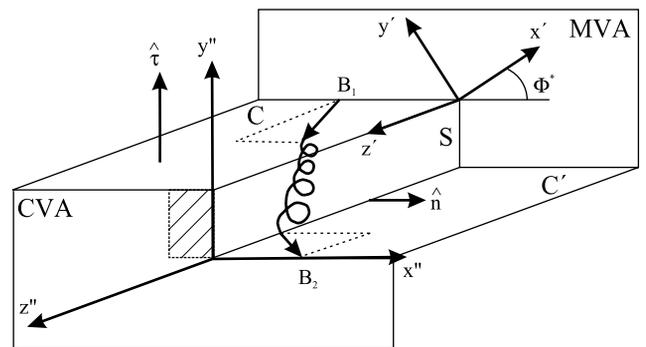


**Figure 3.** Isometric drawing of the geometry of magnetic tubes of force at a slow shock layer (S) for the purpose of illustrating the issues with MVA coordinate system $(x', y', z')$ and the newly proposed CVA coordinate system $(x'', y'', z'')$ for time series where it is suspected that the vector field is coplanar, as in a shock. The normal **n** to the shock and to the coplanarity plane $\tau$ is indicated. The equivalent planes (MVA), (CVA) spanned by eigenvectors of potentially degenerate eigenvalues are also indicated. The split coplanarity plane is labeled C and C′.

system that $\langle B_{y''} \rangle = 0$, where the angular brackets imply the time average. In general there must be changes in a CWD in the remaining transverse direction we will call $\mathbf{z}''$; there is current perpendicular to this polarization plane either in the shock front (S) or throughout the wave train. Like the component along the wave vector, the magnetic component of the CWD out of the coplanarity (polarization) plane are ideally not only expected to be constant but zero. By the same argument that motivated MVA as a minimization problem, the variance of the components out of the coplanarity plane should also be small for a CWD.

[16] Therefore to find a geometry suitable for CWDs, a coordinate system must be found where both $\sigma_x''$ and $\sigma_y''$ are small while $\langle \mathbf{B}(t) \rangle \cdot \mathbf{y}'' = 0$. The first two of these requirements explains how MVA can fail to obtain good CWD normals; a CWD possesses two (!) "minimum" variance directions, presenting two orthogonal directions of "essentially" the same very small variance. For shocks whose internal structure is sensed, and as Figure 3 illustrates, there is a small net average value of $\langle \mathbf{B}(t) \rangle \cdot \mathbf{y}''$ [*Goodrich and Scudder*, 1984; *Tidman and Krall*, 1971] that will cause slight errors to be made on requiring the chosen CVA coordinate system by enforcing $\langle \mathbf{B}(t) \rangle \cdot \mathbf{y}'' = 0$. Depending on the fraction of data included in the time series containing the current layer, there may be a slight preference for a lower variance along the normal relative to the $\mathbf{y}''$ direction. Offsetting this possibility are 2-D effects that impact the constancy of the normal component and preshock and postshock wave trains that contribute to both variances, leaving it a tossup which directions (normal or along coplanarity normal) that should have the lesser variance.

[17] Figure 2d depicts a fast shock magnetic field profile (as a concrete example of a CWD) in the spacecraft frame, using the same colors as the other panels for its x (cyan), y (red), and z (green) components. In this frame there is usually variance along all three Cartesian directions. Figure 2e illustrates the MVA reorganization attempted for the shock time series and variances. The FOM values are comparable to one another, unlike the situation in Figure 2b where the RD FOM were distinct in the ratio exceeding 8. The ratio of eigenvalues is 2.7, well below the recommended value of 10 for confident geometry inversion. The minimum variance red (x') and cyan (y') traces have mean values both substantially different from zero.

[18] However, Figure 2f illustrates the reorganization afforded by the CVA technique developed below. The new x (red) trace is steady, while the cyan trace reflects $\langle \mathbf{B}_{y''} \rangle = 0$. The $\mathbf{z}''$ component of $\mathbf{B}$ increases in time, and this profile is recognized as a potential shock candidate. CVA has found the "correct" underlying shock solution, while MVA has not. The FOM for CVA is the variance along the newly selected $\mathbf{x}''$ and $\mathbf{y}''$ directions divided by the invariant Pythagorean sum of variances. The FOM are approximately equal and more equal than the FOMs for the MVA assay of the same time series in Figure 2e. The separate totals of the FOMs from MVA and CVA for the same time series are, by construction, equal; the CVA choice has enforced coplanarity at the price of slightly increasing the variance along the selected normal. The equipartition of the FOM at small values in CVA is noteworthy, since as we see here it correctly suggests a CWD, affirming the geometrical construction of CVA is more than linear algebra. As shown below when the CVA is applied to modeled TDs, the equipartition of its FOMs is not proscribed by the technique but a diagnostic of the technique's suitability for the type of time series under study.

[19] An interesting question remains with real data, "How does one tell whether one should stop at the MVA or the CVA geometry inversion?" A clue is in the MVA FOM after MVA reorganization of time series with different intrinsic symmetries: Figures 2b (RD) and 2e (Fast Shock). The MVA FOM on the RD are distinct with ratio 8+, clearly well separated on the interval of [0,1]. By contrast, the MVA FOM for the shock layer has ratio 2.7 in Figure 2e; while formally distinct, these FOM are operationally small and their ratio well below 10 recommended for accurate geometry inversions using MVA at elliptically polarized layers. If the MVA situation on a new time series looks like that in Figure 2e, it is appropriate to press on with CVA analysis developed in this paper. The price of not pursuing this distinction can leave the physics of the layer unfocussed, as in upper three panels of Figures 6 and 7, where data CWDs placed in MVA coordinates are not recognizable even as members of the DDs of MHD.

[20] To shed further light on this problem, we complete our graphical discussion in Figure 2c, where the "linear polarization" tool of CVA analysis has been blindly used on an elliptically polarized layer of a simulated RD. In seeking to enforce a CWD geometry, this procedure has increased the variance in CVA along the suggested normal (cyan) trace FOM(1), giving to it nearly all the very substantial variance that previously was along the $\mathbf{y}'$ direction in MVA. By the nature of CVA, the $\mathbf{z}''$ axis in CVA is the same physical direction as in MVA, so the particular "reconstruction" in Figure 2c selected by the CVA algorithm has effectively mixed the x' and y' MVA components en route to satisfying the CVA algorithm. It is not so damaging that CVA $Q_1$ is preferentially increased by CVA in Figure 2c; rather, it is that by performing CVA blindly on the time series that a large ratio of eigenvalues is inverted upside down for CVA FOMs with the implication that in CVA the variance along the normal is 8+ times the variance in the direction normal to the coplanarity plane. The clear indication that CVA is inappropriately applied in this time series is that $Q_1$ in CVA is comparable to $Q_2$ of MVA on the RD, which we have already said was clearly distinguishable from and 8+ times larger than $Q_1$. The fact that CVA $Q_1$ is not substantially the same as CVA $Q_2$ implies that the CVA geometry is unlikely to be correct. Conversely, in Figure 2f, when the final result and correct geometry for the shock simulation was acquired by CVA, $Q_1,Q_2$ were essentially the same, even though the algorithm described below does not enforce this condition (as can also be seen in Figure 2c).

## 4. Geometry for the CWD Problem

[21] The eigenvector $\zeta_3$ associated with the maximum eigenvalue of the MVA's covariance matrix is the most robust eigenvector for either the RD or shock layers even in the presence of 2-D effects and even when $Q_2/Q_1 \ll 10$ (cf. statistical study summarizing over 100,000 MVA inversions [*Scudder et al.*, 2005a]). While this is also true in the situation as $\omega > 30°$, CVA is not recommended for geometry

reconstruction in DDs with such shallow deflections. In CVA we identify $\zeta_3$ with the direction transverse to the normal (wave vector) and parallel to the components of **B** that participate in the net compression at the shock (undulations in the CWD). Such an eigenvector will be oriented in the phase front of a shock (S), transverse to the normal and in the coplanarity plane parallel to C, C' of Figure 3. In the CVA, $\mathbf{z}'' = \zeta_3$ will be the same maximum variance eigenvector $\mathbf{z}'$ found via MVA. Since the $B_{z''}$ possess a net change at a shock wave, its variance will certainly be nonzero and expected to be the direction of the largest variance for a CWD (as shown for a shock in Figures 3e and 3f).

[22] The normal $\tau$ to the coplanarity plane (Figure 3) is required to be perpendicular to $\zeta_3 = \mathbf{z}'$, yielding the first CVA condition; (1) $\tau \cdot \zeta_3 = 0$. Since on average **B** must reside in (be parallel to) the coplanarity plane, we obtain the second CVA condition: (2) $\tau \cdot \langle \mathbf{B} \rangle = 0$. As we require a unit $\tau$ vector, we enforce the third CVA condition: (3) $|\tau|^2 = 1$. These three conditions determine all components of $\tau$ to within an unimportant overall sign. The shock normal is then given by $\mathbf{n} = \tau \times \zeta_3$, completing a new right-handed CVA coordinate system: $\zeta_1' = \mathbf{n}$; $\zeta_2' = \tau$; $\zeta_3' = \zeta_3$. The matrix of transformation from the original to the CVA coordinate system is given by

$$\overset{\leftrightarrow}{L} \, (\text{original} \rightarrow \text{CVA}) = \begin{pmatrix} n_x & n_y & n_z \\ \tau_x & \tau_y & \tau_z \\ \zeta_{3x} & \zeta_{3y} & \zeta_{3z} \end{pmatrix}$$

so that the transformed magnetic field would be obtained by matrix multiplication as $\mathbf{B}_{\text{CVA}} = \overset{\leftrightarrow}{L} \cdot \mathbf{B}_{\text{original}}$. This transformation implements in one step, a procedure that is essentially two steps in succession: transforming to MVA followed by a rotation by an angle $\varphi^*$ about $\zeta_3$ to achieve the average coplanar condition.

## 5. Discussion

[23] The geometrical content of the rotation involving $\varphi^*$ (implicit in the top two rows of **L** above) is illustrated in Figure 3. In the plane (labeled MVA) the typical orthogonal MVA eigenvector directions $\mathbf{x}'$, $\mathbf{y}'$ found for a shock are indicated. Because of the near degeneracy of the minimum and intermediate eigenvalues, these coordinates are not uniquely constrained and could be essentially any pair of perpendicular directions in this plane. In the case of strict eigenvalue degeneracy the actual vectors selected are algorithm-dependent! Instrumental circumstances as well as other perturbations on the data may "split" the degeneracy presented by the idealized DD. This is generally of no consequence except when a recipe depends on the uniqueness of a direction assigned to one of these two directions as with MVA normals. By contrast to MVA, the choice of $\varphi^*$ corresponds to picking two other equally viable perpendicular directions, $\mathbf{x}''$ and $\mathbf{y}''$ (front plane in Figure 3 labeled CVA) that span the same plane as did $\mathbf{x}'$, $\mathbf{y}'$ by requiring the $\mathbf{B}''$ in CVA to be coplanar on average.

[24] A nonzero choice of $\varphi^*$ implies that "the" normal according to CVA, $\zeta_1'$, is no longer the strict minimum variance direction of MVA, $\zeta_1$. In fact, the algebraic construction of $\overset{\leftrightarrow}{L}$ above illustrates that there is no room for an additional minimization of the variance along the normal once the maximum variance direction has been

adopted as one of the basis vectors of the CVA system. This also shows that there is no recipe with Lagrange multipliers and minimization that can find the CVA basis, since it is not strictly a direction of minimum variance. There may be a minimization formulation for CVA that asks the variance along two orthogonal directions $\mathbf{n}'$, $\tau'$ to be maximally equal, with the third basis vector found by the right hand rule. Were such directions found, the litmus test of such a technique would be how far $\mathbf{n}' \times \tau'$ was from being parallel to the direction of maximum variance that is robustly determined and probably the best vector available for geometry at such layers when only using one vector field.

[25] As shown in the examples in Figures 2d–2f, the variance $Q_1$ of the field components along the CVA "normal" for shocks remains small because the variance along any direction in the plane labeled MVA/CVA of Figure 2 is small, bounded by theorem by the sum of two assumed smallest eigenvalues of the covariance matrix. The precondition for attempting the reorientation of the normal by the CVA procedure was that the data set does not determine it very well, and that $Q_1$, $Q_2$ are both "small" and not so far dispersed obeying $Q_2/Q_1 \ll 10$. (Common sense must enter these decisions, especially when enforcing the eigenvalue ratio tests between eigenvalues that are small and when either value is computed to be below the real noise floor of the measurement.) In a sense we are hypothesizing the existence of the coplanarity plane in place of presuming that the direction of minimum variance always defines the current sheet normal. The maximum variance direction and the CVA coplanarity direction once found in a CWD then determine a better normal (see below for simulations of precision) via the right-hand rule, provided the CVA FOM are consistent with the CVA hypothesis.

[26] Conversely, as shown in Figure 2c, when CVA is forced on a RD time series, the result is to put a large $Q_1$ on $\zeta_x'$ components in order to make the $\zeta_y'$ components have zero mean; this is not a failure of CVA but of judgment about the distinctness of the eigenvalues of MVA that implies that the MVA eigenvectors, not CVA basis, should have been used to determine the geometry.

[27] The sieve between CVA and MVA geometry then devolves on the judgment of the effective degeneracy of the smallest two eigenvalues of covariance matrix and reviewing the figures of merit of both approaches to see which techniques presumptions may have been contradicted. Two Figures of Merit, FOM = $Q_1$, $Q_2$, should be considered. Notice that the FOM goes with the process and the time series. The success of MVA requires that $Q_2 > 10Q_1$, as is almost satisfied in Figure 2b. Clearly, when FOM = $(10^{-4}, 0.4, 0.5999)$, MVA (CVA) does (does not) give a reasonable geometrical reconstruction for the normal, but not a terribly precise idea even of the direction of maximum variance. (Since TD and RD properties are not tied to the absolute direction of the intermediate or maximum eigenvector this degeneracy is unimportant.) However, when FOM = (0.04, 0.1, 0.86), CVA (MVA) can (cannot) provide a viable geometry for physical interpretation.

### 5.1. Can CVA Get Confused While Analyzing TDs?

[28] It has been argued during the refereeing of this paper that CVA is fatally flawed and would misconstrue TDs as

shock waves. This argument originates with the fact that TD magnetic vectors are indeed coplanar, a perceived similitude between CWDs and TDs. This section is designed to refute this seemingly cogent criticism.

[29]   (1) It is undisputed that the coplanarity plane of a TD is parallel to the planar current sheet of the TD; the TD coplanarity normal and the normal to the current sheet of the TD are parallel. (2) It is also an undisputed fact that the Rankine-Hugoniot conditions and the definition of a plane-polarized wave imply that the CWD coplanarity plane contains the wave vector, which is the normal for a 1-D CWD. (3) Point 2 implies that the normal to the CWD coplanarity plane is orthogonal to the normal/wavevector of the CWD, in contradistinction to the geometry of the TD's coplanarity plane. (4) Points 1 and 3 imply that for a TD, only one direction is expected to have a constant ($\sim$0) magnetic field component; as a corollary, a TD is expected to have only one direction of small variance, since it has only one a priori direction where a component of **B** is expected to be constant. (5) By contrast, point 3 also implies that two orthogonal projections of **B** at a CWD should be constant, with one of them being zero; both such components should have small variance. Thus a CWD (TD) does (does not) have the degenerate eigenvalue situation that CVA presumes. Used properly to test the CWD hypothesis, CVA would repudiate a TD time series as consistent with a CWD, in spite of the fact that TDs and CWDs each have a coplanarity plane of a different kind.

[30]   As a simple demonstration that the logic of the above response to the referee is correct, a thousand different TDs are analyzed by CVA and MVA using the rules of selection outlined above. The TDs are modeled in the simplified parametric form

$$B_x = 0.02 \sin 20\pi\Theta(t)$$

$$B_y = 2 \cos \omega_o\Theta(t)$$

$$B_z = 5 \sin \omega_o\Theta(t)$$

$$\Theta = \frac{1}{2}\left(1 + \tanh\frac{t - 0.5}{0.25}\right),$$

where $\omega_o$ is the net angular rotation across the current layer. The hodogram is an ellipse and a small amount of noise has been retained along the normal. The thousand TDs differed only by the size of $0 < \varepsilon < \omega_o < \pi$. Figure 4 summarizes the variation of the FOM variations of the two techniques. In the solid curve the variation of $\Psi_{CVA} = ((FOM_{CVA}(1))/(FOM_{CVA}(2)))$ from CVA is plotted, while the red curve depicts $\Psi_{MVA} = ((\lambda_{MVA}(2))/(\lambda_{MVA}(1)))$ from the eigenvalues of MVA. Below $\omega \approx 30°$ these two traces are distinct, but they come together and overlay one another at larger $\omega$. The green vertical line indicates the lower bound of the DD regime ($\omega = 30°$) where geometry is inferable from variance studies. (Note that this lower bound also prevents MVA from "building a geometry" at very small $\omega$s even though the ratio of very small eigenvalues may exceed the suggested ratio of 10. The dark blue highlighted portion of this curve indicates intervals in $\omega > 30°$, where $\Psi_{MVA} > 10$ and MVA is expected to be able to accurately identify the direction of minimum variance without potential confusion. The
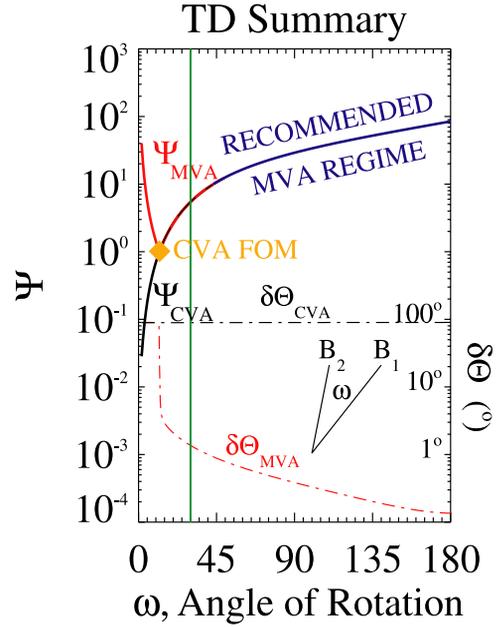


**Figure 4.**   Summary of 1000 TDs analyzed by CVA and MVA techniques. Horizontal axis is the net angle of magnetic rotation, $\omega$. The vertical axis is $\Psi$, the ratio of Figures of Merit (FOMs) defined in the text for CVA in solid curve and MVA in the red curve. At intermediate $\omega$s these two curves become identical. The thick blue curve indicates domain where MVA is said to be a satisfactory tool for the geometry inversion of the (RD/TD) current sheet. Orange diamond indicates the recommended locale where CVA analysis is consistent with expected FOMs of a Coplanar Wave Disturbance (CWD). Thick green line is the $\omega = 30°$ dividing line for "accidental" degeneracy: where the arc of the hodogram in Figure 1 starts to look linear, providing insufficient leverage to extract a geometry by MVA. It should be noted that all attempts for CVA analysis that are anywhere close to acceptable FOM ratio are not in the domain of Directional Discontinuities (DDs) usually attempted for current sheet geometry. The conclusion is that the only acceptable geometries for these TDs would be provided by MVA analysis and that there is essentially zero chance that CVA when processing a true TD would mistake it for a CWD.

orange diamond is located on the single point on the solid curve where $\Psi_{CVA} \approx 1$, the regime where CVA expects to find viable geometry. At all other locations in these simulations of TDs the CVA premise of equal FOMs is repudiated; consequently, its suggested geometry is also of no interest in the physical diagnosis of the time series. Furthermore, the isolated angular regime where there is a suggestion of confusion and equal FOMs happens when $\omega < 30°$, a situation known for over 35 years to be a poor circumstance to determine a DD's geometry. Thus from two vantage points CVA will not misconstrue true TDs as shocks: (1) CWD and TDs have different eigenvalue symmetries and are accordingly distinguishable when corollaries of the premises of these tests are checked; and (2) direct simulations, using the CVA decision framework, clearly rejects DDs
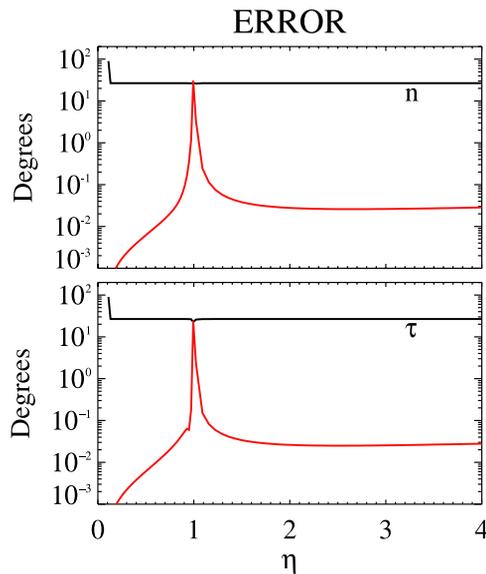
## ERROR



**Figure 5.** Inventory of the precision of recovery of CWD geometry at slow and fast mode shocks as a function of compression ratio $\eta = B_2/B_1$, using MVA (black) and CVA (red). Upper (lower) panel depicts the error in the normal (coplanarity normal) directions from the model. Quantitative demonstration that CVA does an excellent job recovering shock normals and coplanarity directions, while MVA does not.

with $\omega > 30°$ as candidate CWDs, let alone a specific type of (intermediate) shock suggested by the referee. To underscore the precision of MVA in this environment, the dashed red curves of this figure depict the error in the recovered normal to the modeled current sheet (using the scale on the right-hand vertical axis). For MVA above $\omega = 30°$ this error is less than $1°$. For the high eigenvalue ratios with MVA at small $\omega$s the conventional wisdom is upheld with MVA missing the normal by $90°$! By contrast, and as expected, the poor CVA $\Psi_{CVA}$ discussed above correctly presages the $90°$ errors (dotted black line) realized for all $\omega$s when blindly using CVA for the geometry, after ignoring the poor FOM attributes for these TDs. This finding also illustrates that having a reasonable CVA FOM is not enough to go forward with the CVA geometry; rather, good FOMs and $\omega \geq 30°$ are necessary to make a credible argument that the geometry inversion is viable.

### 5.2. Precision of CVA and MVA Geometries at Synthetic Slow and Fast Shocks

[31] A series of one-dimensional magnetosonic shock layers were prepared to contrast the geometry inversion provided by CVA and MVA. The modeled oblique shocks only differ by their compression factor, $\eta = B_2/B_1$, which ranges from $\varepsilon \approx 0$ to 4, from switch-off slow shocks to high mach number fast-mode shock layers. The normal components of shocks of different compression have the same size, leading to a $\Theta_{Bn}$ variation with $\eta$. Noise localized to the layer is superposed and a realistic net value for $\langle \mathbf{B}''_y \rangle$ is in each profile. (The shock profile in Figure 2d was an example from this set.) MVA and CVA were used on the same time series to recover the geometry, which is then compared against the known geometry of the simulated shocks. Figure 5 (top) summarizes the angular error in degrees for the recovery of the shock normal and the coplanarity normal in the bottom panel. The black (red) trace in each panel is the absolute angular error using MVA (CVA). Except in the vicinity of very weak ($\eta \approx 1$) shocks, the CVA approach recovered the shock geometry at better than $0.1°$, while MVA rather systematically got the CWD geometry wrong, missing by more than $25°$. Since CVA explicitly requires a good direction of maximum variance, its "failure" at very weak shocks is understandable, since there is little leverage in the very small transverse change in that negligible circumstance.

### 5.3. Observations
#### 5.3.1. Plane-Polarized Wave Disturbance

[32] As the first of two brief examples using this technique, we consider GGS-Polar magnetometer data on 31 January 2004, which contains a magnetopause crossing discussed more extensively in two recent papers [*Mozer et al.*, 2004; *Scudder et al.*, 2005b]. The upper three panels of Figure 5 are the three components of **B** in the MVA coordinate system determined from data between the vertical dashed lines between approximately 0746:00 and 0748:00UT. The principal axis transformation determined from the MVA procedure produces $\mathbf{B}(t)$ with strongest variations along the $\mathbf{z}'$ axis, and successively less variation along $\mathbf{x}'$ and $\mathbf{y}'$, but both of these MVA components have significant average components across the analysis interval. The MVA FOM are $Q_1 = 0.039$, $Q_2 = 0.115$, with a ratio of $2.9 \ll 10$. Each of the MVA FOM is strongly smaller than $Q_3$. Since they are not large relative to one another, "the" minimum variance direction is not well defined.

[33] The small and comparable sizes of the MVA FOM suggest considering CVA for the geometry of this disturbance as a CWD. The lower three panels illustrate the field transformed to the CVA system. The average of the $\mathbf{y}''$ component of $\mathbf{B}_{HVA}$ is zero with only modest variations, while $B''_x$ is remarkably steady. The CVA FOM are nearly balanced with values $Q_1 = 0.075$, $Q_2 = 0.079$. This interval is consistent with being a CWD, a viewpoint not accessible from the MVA reorganization in the upper three panels. The planar wave field is consistent with a linearly polarized large-amplitude slow-mode wave. The wave is slow mode by showing that the density and magnetic field strength are anticorrelated [*Scudder et al.*, 2005b].

#### 5.3.2. Candidate for Slow Shock

[34] A second example in the same format is shown in Figure 6 where an abrupt reorientation of the field is seen about 0745:57UT. The magnetic field transformed to the MVA geometry determined for the interval between the vertical dashed lines is shown in the upper three panels, while the CVA geometry inversion is illustrated in the lower three panels. The MVA FOM are $Q_1 = 0.049$, $Q_2 = 0.184$, small and close together with ratio $3.7 \ll 10$. The magnetic field organized in MVA has a strong average $\mathbf{y}'$ component. In keeping with our arguments above, the MVA geometry is not warranted. The CVA approach finds a candidate coplanarity plane with CVA FOM of $Q_1 = 0.126$, $Q_2 = 0.107$ that are nearly balanced, as we saw in Figure 2f in our simulations with a CVA recovery of a CWD. The physical interpretation in the MVA system is confused at best, while
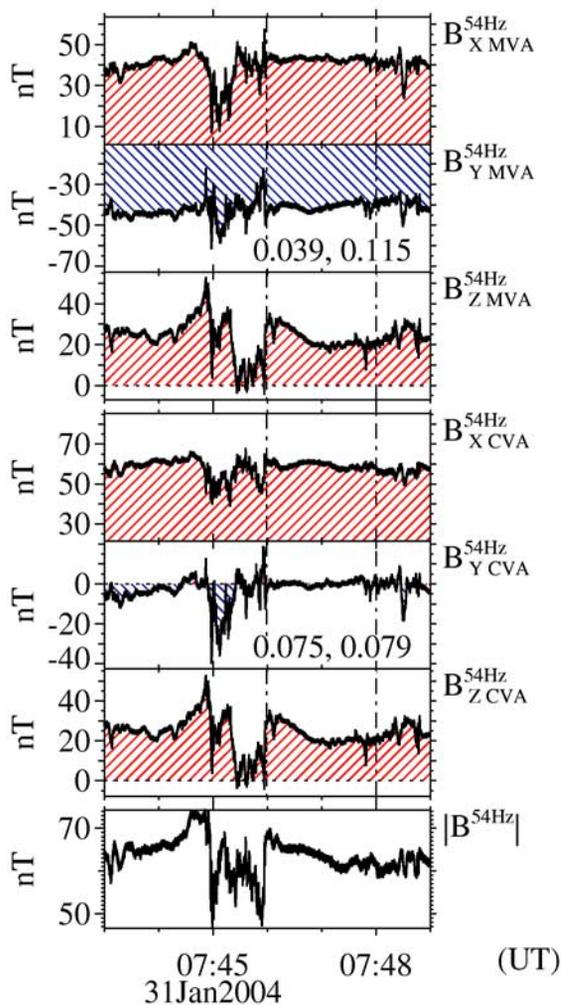
**Figure 6.** GGS Polar data for 31 January 2004 contrasting the magnetometer data at the Earth's magnetopause in MVA versus CVA coordinate representation. Lower three panels consistent with the detection of a linearly polarized slow mode wave.

in CVA this interval is consistent with a CWD with a relatively sharp field magnitude change within it. Of particular interest is the planar structure with a nearly complete "switching-off" of the transverse $B_z''$ component, reminiscent of the behavior of the strongest (switch-off) slow shocks.

[35] A successful ($Q_1 \approx Q_2$) CVA geometry does not prove that the time series is a shock but indicates that the time series has passed a falsifiable test consistent with a planar vector field. A possible reason for this planar condition (especially in the presence of the abrupt change in the $z''$ component) is that this is a shock layer; this hypothesis is fully explored by *Scudder et al.* [2005b].

## 6. Summary

[36] CVA performs well with high precision on simulated and real data and should actively be considered for geometrical reconstructions in tandem with MVA techniques. In the framework of hypothesis testing, MVA is best adapted to answering the question "Is it a 1-D current layer

possessing elliptical polarization," while CVA is best adapted to answering the question "Is it a 1-D current layer with linear polarization." Explicit demonstrations have been provided to show that MVA works poorly for CWD and CVA works poorly for RDs/TD. MVA and CVA, together with their figures of merit, can be used to test these two hypotheses; failing both these hypotheses also provide a rationale for a category of "other" shear layers of possibly multidimensional character that should not be interpreted as if they were one-dimensional transects. In this way physical models can be evaluated in the best geometries that can be determined from the limited world line data that satellites provide. The community deserves a defense of the coordinate systems proffered to interpret data. The FOMs indicated should be used and presented to substantiate the use of a reordering coordinate system. It should be unacceptable practice to present data in MVA or CVA without a demonstration of their relative plausibility and consistency of the FOMs with the premises that generate the mathematics that yield the coordinate transformation recipes.
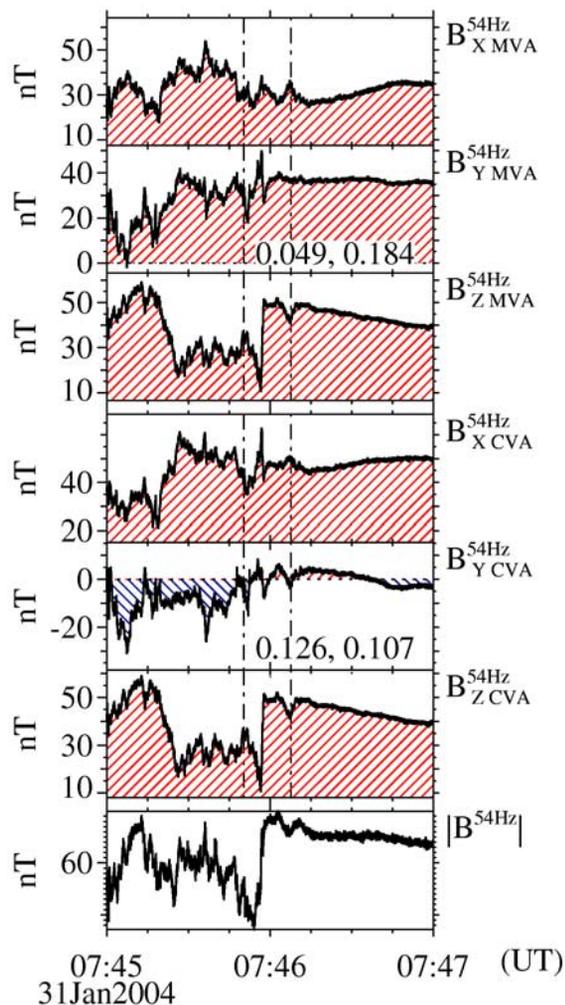


**Figure 7.** Polar data for 31 January 2004 contrasting the magnetometer data at the Earth's magnetopause in MVA versus CVA coordinate representation, illustrating the detection with CVA of a candidate for plane-polarized disturbance.

[38] Lou-Chuang Lee thanks Jih Kwin Chao and another reviewer for their assistance in evaluating this paper.

## References

Arfken, G. B., and H. J. Weber (2001), *Mathematical Methods for Physicists*, 5th ed., 596 pp., Elsevier, New York.

Baumjohann, W., and R. A. Treumann (1996), *Basic Space Plasma Physics*, Imperial Coll. Press, London.

Burlaga, L. F., J. F. Lemaire, and J. M. Turner (1977), Interplanetary current sheets, *J. Geophys. Res.*, *82*, 3191.

Goodrich, C. C., and J. D. Scudder (1984), The adiabatic energy change of plasma electrons and the frame dependence of the cross shock potential at collisionless magnetohydrodynamic shock waves, *J. Geophys. Res.*, *89*, 6654.

Knetter, T., F. M. Neubauer, T. Horbury, and A. Balogh (2004), Four-point discontinuity observations using Cluster magnetic field data, *J. Geophys. Res.*, *109*, A06102, doi:10.1029/2003JA010099.

Mozer, F. S., S. D. Bale, and J. D. Scudder (2004), Large amplitude, extremely rapid, predominantly perpendicular electric field structures at the magnetopause, *Geophys. Res. Lett.*, *31*, L15802, doi:10.1029/2004GL020062.

Scudder, J. D. (1995), A review of the physics of electron heating at collisionless shocks, *Adv. Space Res.*, *15*, 181–223.

Scudder, J. D., Z. W. Ma, N. Omidi, and P. Puhl-Quinn (2005a), World line dependence of current sheet normal inferred by minimum variance techniques, *J. Geophys. Res.*, doi:10.1029/2004JA010661, in press.

Scudder, J. D., Z. W. Ma, and F. S. Mozer (2005b), Debye length structures in Earth's reconnection layer: Observations and simulations, *Phys. Plasmas*, in press.

Sonnerup, B. U. O., and L. H. Cahill (1968), Explorer 12 observations of the magnetopause current layer, *J. Geophys. Res.*, *73*, 1757.

Sonnerup, B. U. O., and M. Scheible (1998), Minimum and maximum variance analysis, in *Analysis Methods for Multi-Spacecraft Data*, *Sci. Rep. SR-001*, edited by G. Paschmann and P. W. Daly, p. 185, Int. Space Sci. Inst., Bern, Switzerland.

Tidman, D. A., and N. A. Krall (1971), *Shock Waves in Collisionless Plasmas*, Wiley-Interscience, Hoboken, N. J.

Vinas, A. F., and J. D. Scudder (1986), Fast and optimal solution to the "Rankine-Hugoniot Problem," *J. Geophys. Res.*, *91*, 39–58.

―――――――――――

J. D. Scudder, Department of Physics and Astronomy, University of Iowa, Room 203 Van Allen Hall, Dubuque at Jefferson Streets, Iowa City, IA 52242-1479, USA. (jack-scudder@uiowa.edu)